Molecular simulation of a reverse osmosis polyamide membrane layer. In silico synthesis using different reactant concentration ratios

Xuefan Song, Jean-Marie Teuler, Wafa Guiga, Claire Fargues, Bernard Rousseau

Molecular simulation of a reverse osmosis polyamide membrane layer. In silico synthesis using different reactant concentration ratios

Xuefan Song[a,b], Jean-Marie Teuler[b], Wafa Guiga[c,a], Claire Fargues[a], Bernard Rousseau[b,*]

October 20, 2021

[a]Université Paris-Saclay, INRAE, AgroParisTech, UMR SayFood, 91300 Massy, France
[b]Université Paris-Saclay, CNRS, Institut de Chimie Physique, UMR 8000, 91405 Orsay, France
[c]Le Cnam, UMR SayFood, 75003 Paris, France
*Corresponding author. Tel.: +33 169153030. E-mail address: bernard.rousseau@universite-paris-saclay.fr. Full postal address: Institut de Chimie Physique, Bâtiment 349, Université Paris-Saclay, 91405 Orsay Cedex, France.

Abstract

We use molecular dynamics simulations at the atomistic level to build a model of aromatic polyamide polymer used in reverse osmosis membranes, from a mixture of *m*-phenylene diamine (MPD) and trimesoyl chloride monomers (TMC). Our purpose is to use different MPD to TMC ratios to reproduce the compositional depth-dependence observed experimentally during interfacial polymerization. MPD to TMC ratios in the range 1:4 to 5:1 have been employed. Reproducibility of the polymerization algorithm is thoroughly studied through the building of several samples under identical conditions. We notice that simulation time of a few microseconds are necessary in order to reach equilibration. We show that the initial monomer ratio has a strong influence onto the final polymer composition and different chemical structures have been created. Large differences are seen concerning cross-linking degree and remaining un-reacted groups. Comparison with available experimental data show that samples built using intermediate values of the MDP to TMC ratio closely resemble aromatic polyamide membranes. We conclude that the simulated samples created under different local concentrations can describe properly the chemical heterogeneities observed experimentally in reverse osmosis membranes.

Keywords: Molecular dynamics simulations, reverse osmosis membranes, cross-linked aromatic polyamide, membranes chemical heterogeneities, polymerization algorithm

1. Introduction

Membrane-based treatments and especially reverse osmosis (RO) are extensively used for pure water production and industrial wastewater treatment, due to advantages such as continuity, easy scaling-up, minimum consumption of chemicals and absence of toxic by-products through this process [1, 2]. As a result, RO occupies more than 50% of seawater desalination market [3]. It is also implemented for the treatment of effluents in order to achieve water reuse in various industrial fields, such as plating industry [4], textile industry [5] or sugar and distillery industry [6]. Its broad applicability in industrial wastewater treatment includes the removal of trace levels of micro pollutants, such as pharmaceutical compounds [7, 8] and pesticide residuals [9, 10, 11, 12].

RO membranes are thin film composite materials and typically consist of a thin layer of cross-linked aromatic polyamide (APA), with a thickness of the order of 150 nm, a microporous polysulfone (PSf) or polyethersulfone (PES) support ($\approx$ 20-50 μm) and a polyesther backing fabric ($\approx$ 100 μm). The active layer, *e.g.* the separating region of the membrane, is the APA layer. It is obtained using interfacial polymerization between *m*-phenylene diamine (MPD) and trimesoyl chloride (TMC) monomers. In commercial membranes manufacturing, the microporous support [13] is impregnated with an aqueous solution of MPD monomers and placed in contact with an organic TMC solution. Several groups also succeeded in obtaining *free-standing* membranes where polymerization takes place directly at the aqueous/organic solvent interface. In both cases, chemical reactions occur as MPD monomers dissolve into the organic phase. The process is thus controlled by solubility and diffusion of MPD monomers into the latter phase. As polymerization takes place, the medium changes drastically with the formation of the membrane and the process becomes even more complex. As presented in a very recent review by Habib and Weinman [14], many parameters can influence the synthesis process and the final properties of the membrane. The presence and nature of a supporting layer, MPD and TMC concentrations, reaction time, temperature, additives are amongst the most important parameters. Chai and Krantz [15] demonstrated that for very small TMC concentrations, the interfacial polymerization is controlled by species diffusion in the organic layer, while for higher TMC concentrations appropriate to commercial practice, the process is controlled by MPD diffusion in the interfacial polymerization film layer. Dutta *et al.* [16] noticed that the diffusivity of MPD monomer from

the aqueous to the organic phase is the important factor regarding the uniform composition and morphology of the polymer formed. Excess of one of the monomers may lead to an inhomogeneous concentration of carboxylic group or amine group along the membrane thickness. Khorshidi [17] also demonstrated the importance of the MPD/TMC ratio on the final aspect of the membrane, obtaining thin polyamide layer with nodular structures or looser APA layer with a ridge-and-valley structure. By changing the MPD/TMC ratio, Xu *et al.* [18] were able to optimize both water permeance and sodium chloride rejection. From a fundamental point of view, there is a need for a deeper understanding of the relationship between synthesis protocol and membrane structure and between membrane structure and separation performances. Molecular simulation tools have been increasingly employed in recent years to elucidate and quantify atomistic scale mechanisms and processes in functional membrane materials [19, 20]. However, because of time and length scales limitations, molecular simulations must be used with caution to screen the influence of various input parameters. *In silico* synthesis of a realistic active APA layer that can reproduce specific experimental properties is, in itself, a challenging task.

Different strategies have been set-up to build APA molecular models. Some groups start with linear chains made from MPD and TMC monomers which are further cross-linked by adding and connecting MPD monomers with free acyl groups [21, 22, 23, 24, 25, 26]. Others directly connect a set of MPD and TMC monomers [27, 28, 29, 30] randomly placed in the simulation box. Some groups also take advantage of a coarse-grained representation of the monomers and of their reaction products to speed up the process and study the kinetics at sight during the membrane formation [31, 32, 33]. In some specific cases, atomic scale membranes can be recreated from the final coarse-grained representation [33].

The majority of these researches focused on methodological aspects of membrane building through molecular simulation [21, 31, 30], water and salt localizations and diffusion mechanisms inside the membrane [21, 22, 27, 23, 26, 34, 28, 35, 36], organic molecules diffusion and foulant model interactions with the APA layer [24, 25, 29, 37, 38, 39, 40]. In most cases, a single molecular simulation box or a few replica are built. The initial conditions are strongly inspired by macroscopic properties given for the FT30 active layer, *i.e.* an hydrated density of 1.38 g/cm^3 and a water content of 23 w% [21] corresponding to a dry density of 1.06 g/cm^3. These data have been discussed by Zhang *et al.* [41]. The authors measured a different water content and consequently a different dry membrane density, around 1.24 g/cm^3. Also, for most of the contributions presented above, simulation boxes are equilibrated for a few tens of ns.

Using large scale molecular simulations, Muscatello *et al.* [33] employed a procedure that mimics experimental interfacial polymerization of TMC and MPD monomers. They studied membrane formation using three different MPD to TMC ratio: 1:1, 3:2 and 3:1. They observed that interfacial polymerization reaction is self-limited and that simulated membranes display a thickness of 5–10 nm. However, no systematic variations of carboxylic and amine group fractions are observed with the initial monomer concentration ratio. To our knowledge, Suzuki *et al.* [42] realized the first systematic study on APA film heterogeneity. They applied an hybrid Monte Carlo/Molecular Dynamics approach to build four different boxes with MPD/TMC ratios 1:4, 1:1, 3:2 and 4:1. Systems with different chemical structures are thus obtained. However, little information is given in terms of structural information or macroscopic properties. In this work, we assume that the compositional depth-dependence observed by several authors [16, 17, 18] is caused by different local MPD/TMC concentrations during the reaction steps. Our purpose is to build several samples starting from different MPD/TMC ratios, to investigate their influence on the chemical structure, local and macroscopic properties and finally relate those data to real systems.

The article is organized as follows. In section 2, we present the methodology used, the systems studied and a new set of chemical descriptors to analyze our samples. In section 3, we validate the methodology and give a detailed description of our samples. In section 4, we discuss the relationship between simulated and real systems. Section 5 contains concluding remarks.

2. Methodology

2.1. Molecular simulation tools

The choice of the force field (FF), which describes physical interactions between particles, is crucial if realistic behavior and quantitative data are expected. Many different FF have been used to study APA membranes including CVFF [43], CHARMM [44], AMBER [45], GAFF [46] and OPLS-AA [47] force fields. As mentioned by Ridgway *et al.* [20], similar behaviors have been reported with these different models. To our knowledge, the work by Liyana *et al.* [30] is the only one where different force fields were compared using the same building methodology: for the three force fields studied, TraPPE [48], OPLS-AA, and GAFF, the average hydrated densities of the membranes are in very good agreement.

In this work, we used the OPLS-AA force field [47]. The OPLS-AA parameters were opti-

mized to fit experimental properties of liquids, such as density and heat of vaporization. Free energy of hydration of organic molecules using the TIP4P model [49, 50] is also an important component of the optimization process. This makes it a good candidate for the study of APA membranes, in presence of water (TIP4P model) and other organic components.

Molecular simulations were realized using the Lammps Molecular Dynamics Simulator (Lammps, August 2018 version) [51, 52]. Initial box configurations, as well as input files for Lammps simulations were created using our local molecular dynamics simulation package, Newton [53]. We wrote a set of scripts and codes to control the polymerization steps, based on Lammps functionalities (see the simulated polymerization section 2.2 for details).

During molecular dynamics simulations, a Lorentz-Berthelot combining rule is used for Lennard-Jones interactions between unlike particles with a cut-off distance of 10 Å and tail corrections. Long-range electrostatic interactions were calculated with the particle-particle particle-mesh Ewald solver [54], with a 10 Å real space cut-off distance and a reciprocal space relative accuracy of 10^{-4}. The equations of motion are based on Nosé-Hoover style Hamiltonian with a time step of 1 fs [55]. Thermostat and barostat use a damping factor of 0.1 and 1 ps respectively. Standard (hydrostatic) and iso-stress NPT simulations were realized using the Lammps keywords `iso` and `aniso`, respectively. Finally, energy minimization steps used the conjugate gradient algorithm with a stopping tolerance for energy equal to 10^{-4} and a stopping tolerance for forces of 10^{-6} force units.

2.2. Simulated polymerization

The simulated polymerization strategy implemented in this work is based on the work by Harder *et al.* [27], with minor adjustments presented here. A schematic of the simulated polymerization process is given in Fig. 1. The different steps are commented out below. During step 1, a set of n MPD monomers, m TMC monomers and one dimer (to simplify force field handling in Lammps) are randomly placed within a simulation box at the target density of 1.38 g/cm^3 so that monomers stay close enough to each other to facilitate amide bond creation. Following several authors [23, 25, 36], the acyl groups of TMC monomers are hydrolyzed, hence no chloride ions are considered; moreover, TMC monomers are modeled in protonated form [56, 57, 20]. Step 2, the initial system is homogenized during a 30 ns molecular dynamics run in the NVT ensemble at 298.15 K. During step 3, a loop including 150 polymerization attempts is started. Our script `paamaker` searches the smallest distance between the carbon atom of a carboxylic group and

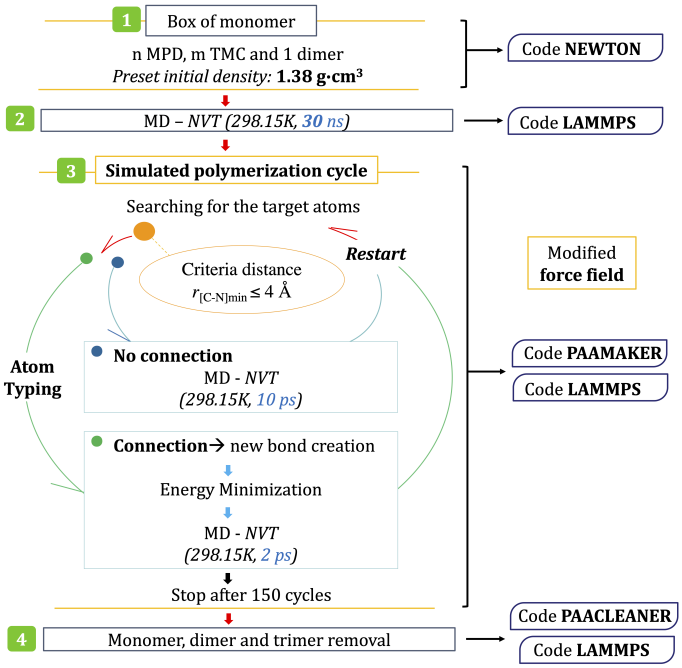

Figure 1: Simulated polymerization algorithm

the nitrogen atom of an amine group. If no such pair is found at a distance smaller than 4 Å, the system is run in the NVT ensemble during 10 ps at 298.15 K. If a pair is found, `paamaker` creates a command file for the Lammps code to form an amide bond by changing atom types, bond, bend, dihedral and improper lists. The amide bond formation is followed by an energy minimization step and by a 2 ps run in the NVT ensemble at 298.15 K using Lammps code. Considering the initial number of MPD and TMC monomers, the amide bond number reaches a plateau before 125 cycles [58]. Finally, during step 4, remaining monomers, dimers and trimers are removed from the simulation box. The polymer is then relaxed and equilibrated using simulations in different statistical ensembles, as described in section 3.1.

During the polymerization process, it was necessary to modify the force field associated with the remaining hydrogen atom on the amide function. OPLS-AA model for this hydrogen atom type is a single positive partial charge. It happened sometimes during the creation of an amide bond that a negative partial charge was brought about too close to the hydrogen atom, creating an infinitely large electrostatic interaction energy, not handled by floating-point arithmetic. To avoid this, OPLS-AA Lennard-Jones parameters from aromatic hydrogen atom types were used for these hydrogen atoms. The repulsion term was then strong enough to avoid the collapse of the partial charges and divergence of the electrostatic energy. Once the polymerization steps ended, the original OPLS-AA force field was recovered. It is worth mentioning here that simu-

lated polymerization algorithms are a crude approximation of the real ongoing processes during interfacial polymerization. The simulated structures have to be compared with experimental data in order to be validated, as will be done in the following sections.

2.3. Description of the studied systems

Interfacial polymerization is realized using an aqueous solution of MPD and an organic solution of TMC. As TMC monomers have a very low solubility in water, the chemical reactions take place in the organic phase as MPD monomers diffuse into it. Typical MPD concentrations in the aqueous phase range from 0.01 to 20.0 w/v % and for TMC in organic phase (mostly *n*-hexane) from 0.001 to 10 w/v % [18, 59, 14]. Depending on specific experimental conditions, authors report MPD to TMC concentration ratios between 1 and 200 [18, 59]. However, MPD concentration in the organic phase can not be easily defined from the knowledge of its concentration in the aqueous phase. It depends on many other parameters such as the monomer partition coefficient between aqueous and organic phases, the diffusion coefficient of MPD in both phases and at the interface or even the presence of additives like triethylamine (TEA). However, simulated polymerization is done without solvent and the most relevant quantity becomes the MPD/TMC monomer ratio. In our simulations, this ratio is expected to represent the local concentration at the chemical reaction location. The ratio used in this study ranges from 1:4 to 5:1 including 1:1 and 3:2 values. The 1:1 ratio corresponds to the stoichiometry of a fully linear chain, while the ratio 3:2 corresponds to a perfectly reticulated APA network. Extreme cases are accounted for using a large excess of TMC monomers (1:4 ratio) or MPD monomers (5:1). Overall, 15 different ratios are used: 0.25, 0.5, 0.75, 1.0, 1.2, 1.3, 1.5, 1.8, 1.9, 2.0, 2.5, 3.0, 3.5, 4.0, 5.0 with an average number of monomers per simulation box of 170. In order to test the repeatability of the simulated polymerization process for these boxes, we created eleven repetition boxes for MPD/TMC ratio of 0.25, 1.5 and 5.0 (see section 3.2 for analysis). This brings to 46 the total number of simulation boxes studied here.

2.4. Chemical descriptors

In order to quantify the chemical structure of our samples and compare with experimental data, we introduce several chemical descriptors related to APA structure already described in [60].

Due to the presence of a 3-functional monomer (*e.g.* TMC), APA polymer exhibits extensive branching and cross-linking leading to a random amorphous structure. It is often represented

as a mixture of two structural units, a linear one and a cross-linked one. These two units are depicted in Fig. 2. The cross-linked unit X appears from the reaction between a TMC monomer and 3 MPD monomers. It is the building block of fully reticulated polymers. Its chemical formula (assuming hydrolyzed and protonated structure) is $C_{18}O_3N_3H_{12}$. The linear unit Y is the building block of fully linear polymers. Its chemical formula is $C_{15}O_4N_2H_{10}$. The cross-

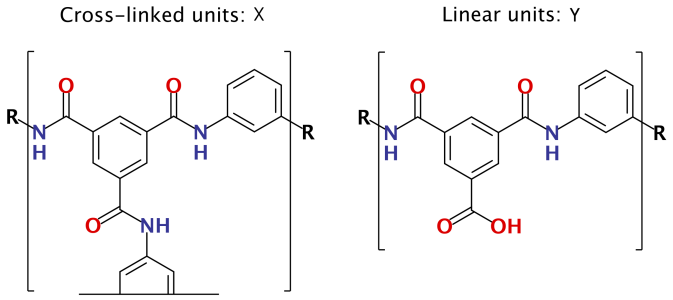

Figure 2: Linear and cross-linked structural units found in APA reticulated polymers.

linking degree, χ, represents the ratio of cross-linked units to the total number of units. It is a quantity that can vary between 0 and 1. It can be expressed as a function of the oxygen to nitrogen ratio, O/N:

$$\chi = \frac{X}{X+Y} = \frac{6}{1+\mathrm{O/N}} - 2\,. \tag{1}$$

For a fully linear structure, the O/N ratio is 2 and the cross-linking degree is zero, whereas for a fully cross-linked structure, the O/N ratio is 1 and χ goes to 1. Elemental analysis can thus provide important informations about the chemical structure of the synthesized polymer. However, this descriptor suffers from several drawbacks. First, it is possible to obtain structures with identical O/N ratio (hence same cross-linking degree χ) but with different oxygen and nitrogen atom fractions. Second, it is assumed that real APA is fully described by units X and Y only. This doesn't account for chain ends as *e.g.* a terminal TMC group with 2 acyl functions or a MPD group with an amine group, and may not be able to describe quantitatively structures with a non negligible amount of such units. In such cases, O/N ratio can have values below one and above two, leading to negative or larger than one cross-linking degree values.

This led us to introduce a new set of four different chemical units, shown in Fig. 3. The units can be seen as *extracted* from a complete APA structure, composed of linear and cross-linked regions plus unreacted amine and carboxylic groups. Unit a corresponds to a TMC monomer

with each carboxylic group replaced by an acyl group. Its chemical formula is $C_9O_3H_3$. Unit b corresponds to a MPD monomer with each amine group replaced by an NH group. Its chemical formula is $C_6N_2H_6$. Unit c corresponds to a terminal hydroxyl attached to a TMC unit a forming one carboxylic group having not reacted. Finally, group d corresponds to terminal hydrogen, attached to a MPD unit b, forming one amine group having not reacted. The acyl groups of TMC units a which are not connected with hydroxyl terminals, form an amide bond with a NH group of MPD units b.

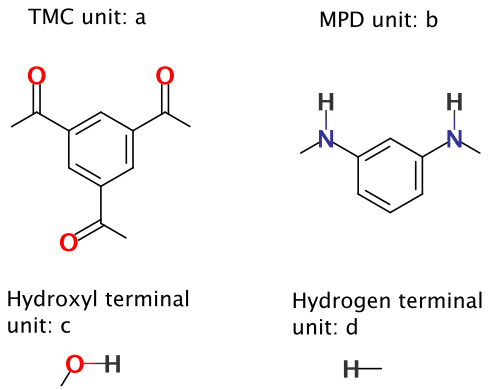

Figure 3: The four chemical units proposed to describe APA polymers.

The total number of atom types in the system can be expressed as a function of the different unit number:

$$\begin{aligned} \mathrm{C} &= 9a + 6b \\ \mathrm{O} &= 3a + c \\ \mathrm{N} &= 2b \end{aligned} \tag{2}$$

The number of hydrogen terminal units is obtained considering that the C=O terminals of TMC units which are not connected with hydroxyl terminal unit $(3a - c)$ form the amide linkage with NH terminals in MPD units not connected with hydrogen terminal units $(2b - d)$:

$$3a - c = 2b - d \tag{3}$$

We now define the connection degree of acyl groups, f_{ac} as the fraction of amide groups to the

sum of amide groups and remaining carboxylic groups after reaction. Using equations 2 and 3, this descriptor can be expressed as a function of C, N and O elements:

$$f_{\mathrm{ac}} = \frac{n_{\mathrm{CONH}}}{n_{\mathrm{COOH}} + n_{\mathrm{CONH}}} = \frac{3a - c}{3a} = 2 - \frac{3\mathrm{O}}{\mathrm{C} - 3\mathrm{N}} \tag{4}$$

This quantity goes to 1 when all acyl groups have reacted to form an amide bond. We proceed the same way for the connection degree of amine groups, f_{am}:

$$f_{\mathrm{am}} = \frac{n_{\mathrm{CONH}}}{n_{\mathrm{NH_2}} + n_{\mathrm{CONH}}} = \frac{2b - d}{2b} = \frac{2\mathrm{C} - 3\mathrm{O}}{3\mathrm{N}} - 2 \tag{5}$$

Finally, the ratio of aromatic rings originating from MPD monomers (*i.e.* with up to 2 amide bonds) to aromatic rings originating from TMC monomers (*i.e.* with up to 3 amide bonds) in the final structure is simply given by the equation:

$$r_{\mathrm{m:t}} = \frac{b}{a} = \frac{9\mathrm{N}}{2\mathrm{C} - 6\mathrm{N}}\,, \tag{6}$$

a quantity called the final MPD/TMC ratio.

From molecular simulations, it is a trivial task to obtain elemental composition. We developped the `paastats` tool to do a topological analysis of our samples in order to identify typical structures like MPD units connected to one or two TMC units and so on; we obtained this information from our simulated samples to check the validity of equations 4, 5 and 6.

In the following, we will compare simulation with experimental compositions. Because hydrogen is not quantifiable by XPS, hydrogen atoms were not accounted for in these computations. Thus, the nitrogen atom fraction is defined as $x_{\mathrm{N}} = \mathrm{N}/(\mathrm{C} + \mathrm{O} + \mathrm{N})$, the oxygen atom fraction is $x_{\mathrm{O}} = \mathrm{O}/(\mathrm{C} + \mathrm{O} + \mathrm{N})$ and $x_{\mathrm{C}} = 1 - x_{\mathrm{O}} - x_{\mathrm{N}}$.

3. Results

3.1. Polymer matrix relaxation and equilibration

At the end of the polymerization steps, the simulation boxes are not equilibrated. Although each amide bond creation was followed by energy minimization and short relaxation using an NVT run, some residual mechanical constraints remain. For example, the diagonal pressure tensor elements for the box with an initial MPD/TMC ratio $r^0_{\mathrm{m:t}} = 1.2$ are very different, ranging from

-250 to 7200 bars. In order to relax these mechanical constraints, a few cycles involving NVT followed by NPT simulations are realized. During NVT simulations, the differences between the pressure tensor elements decrease while the average pressure remains roughly the same. During NPT simulations, the average pressure converges to the target pressure (1 bar) while the box volume changes. After such a few cycles (*e.g.* 2 cycles and 250 ns for the system with $r^0_{\mathrm{m:t}} = 1.2$) small differences still exist between pressure tensor components: $P_{xx} = 215 \pm 50$, $P_{yy} = -58 \pm 100$, $P_{zz} = -132 \pm 50$. At this stage, a long simulation in the NPT iso-stress ensemble is realized in order to relax all pressure tensor diagonal elements independently. The time evolution of the potential energy E_p, the density ρ and box lengths in x, y and z directions, L_i, for system $r^0_{\mathrm{m:t}} = 1.2$ are shown versus simulation time t in Fig. 4.

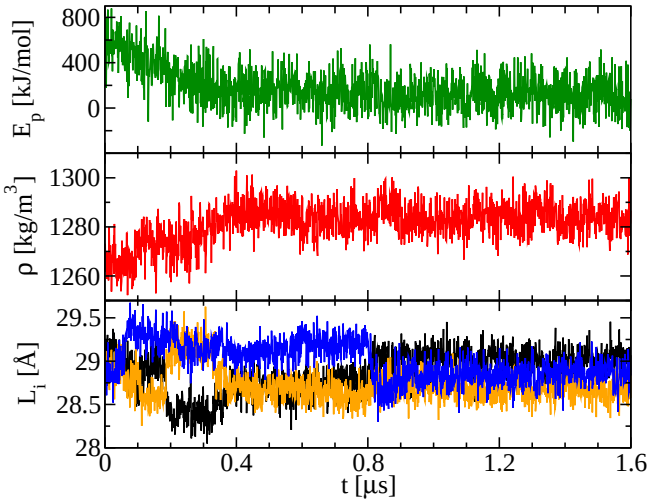

Figure 4: Long time relaxation of the APA box with initial $r^0_{\mathrm{m:t}} = 1.2$. Potential energy E_p, density ρ and box lengths in x, y and z directions, L_i, are shown versus simulation time t. Initial time corresponds to the end of the NVT/NPT cycles. Note that unit of time is in μs.

As can be seen in Fig. 4, the complete relaxation of the simulation box requires quite a long simulation time *after* the end of the NVT/NPT cycles. Over 500 ns are required for the potential energy and the density to converge. The situation is even worse for box length values where abrupt changes, accompanying in most cases molecular conformational changes, are observed. For the system presented here, box length values remain constant after 0.8 μs, although abrupt box length variations are observed up to 3 μs in some boxes. Therefore, in this study, simulation boxes were equilibrated for simulation time as long as 5 μs.

3.2. Repeatability analysis

The simulated polymerization used is a random process. Therefore, it is expected that simulation boxes created under identical conditions will lead to polymers with slightly different structures. This is worsened by the limited number of monomers used. Before proceeding to the study of the influence of the initial MPD/TMC ratio, $r^0_{\mathrm{m:t}}$, it is important to check that our polymer construction process gives equivalent samples under identical conditions.

We created eleven repetition boxes for each of the following $r^0_{\mathrm{m:t}}$ values: 0.25, 1.5, 5.0. Ideally, several repetition boxes should be done for each set of initial condition. However, large computation times impose to reduce the number of boxes studied. At the end of the polymerization process, and after removal of unreacted monomers, dimers and trimers, we did an elemental analysis of the samples in terms of carbon, oxygen and nitrogen atoms from which different descriptors can be obtained. Fig. 5 shows the final oxygen to nitrogen ratio, O/N, oxygen atom concentration, x_{O} and MPD to TMC ratio, $r_{\mathrm{m:t}}$, for the 11 repetition boxes and for each $r^0_{\mathrm{m:t}}$. This set of properties is not fully exhaustive, though we believe it is representative of the chemical nature of the samples. It is clear from Fig. 5 that simulated polymerization is sensitive

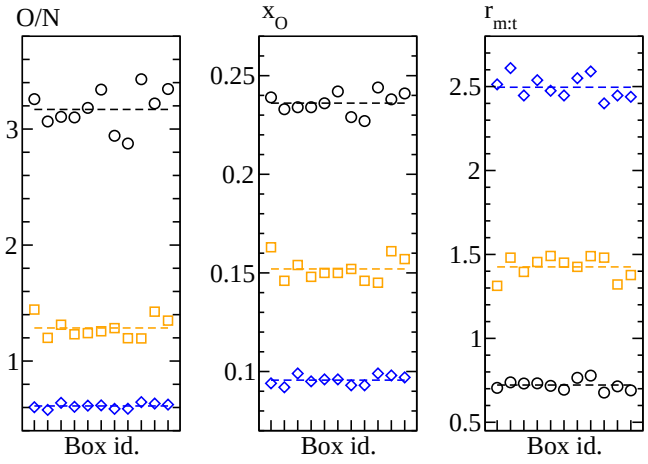

Figure 5: Final oxygen to nitrogen ratio, O/N, oxygen atom concentration, x_{O} and MPD to TMC ratio, $r_{\mathrm{m:t}}$, for the 11 repetition boxes and the different initial MPD/TMC ratio, $r^0_{\mathrm{m:t}} = 0.25$ (circle), 1.5 (square) , 5.0 (diamond). Symbols represent data for each repetition box. Dashed lines are averages over all repetition boxes for a given property and $r^0_{\mathrm{m:t}}$.

to initial conditions. Boxes obtained with different $r^0_{\mathrm{m:t}}$ can be clearly distinguished from each other using O/N ratio, x_{O} and $r_{\mathrm{m:t}}$. For a given $r^0_{\mathrm{m:t}}$, repetition boxes are slightly different and fluctuations are observed for computed descriptors. However, the standard deviations are small

compared with average values and we can assume that each box is representative of the system.

3.3. Systems main trends with $r^0_{\mathrm{m:t}}$

In this section we focus on the main trends observed in our samples for a limited number of $r^0_{\mathrm{m:t}}$ values. Several structural data are given in table 1, averaged over the 11 repetition boxes: N_{mol}, the number of molecules per box; N_{mono}, the number of monomers per molecule; N_{ce}, the number of chain ends per molecule, computed from the number of MPD units b with one amine group plus the number of TMC units a with two carboxylic acid groups; N_{cl}, the number of TMC cross-linked units per molecule, computed from the number of TMC units a connected to three MPD units b with no amine group; the molecular size distribution (expressed in number of atoms per molecule). It is clear from table 1 that two different trends are observed. Samples

$r^0_{\mathrm{m:t}}$	0.25	1.5	5.0
$\langle N_{\mathrm{mol}} \rangle_b$	10.9 ± 0.6	5.6 ± 0.6	21.8 ± 0.7
$\langle N_{\mathrm{mono}} \rangle_b$	6.0 ± 0.2	25.0 ± 3.0	6.4 ± 0.2
$\langle N_{\mathrm{ce}} \rangle_b$	2.05 ± 0.02	6.3 ± 0.8	3.72 ± 0.06
$\langle N_{\mathrm{cl}} \rangle_b$	0.07 ± 0.02	1.9 ± 0.4	0.03 ± 0.01
Size distribution (atoms)			
0-200	1	0.62	0.97
200-500	0	0.193	0.03
500-2000	0	0.187	0

Table 1: Structural characteristics of systems built using different initial MPD/TMC ratios, $r^0_{\mathrm{m:t}} = 0.25$, 1.5 and 5.0. $\langle \rangle_b$ indicates averages over repetition boxes. See text for definition of the different quantities.

synthesized with extreme $r^0_{\mathrm{m:t}}$ values (*i.e.* $r^0_{\mathrm{m:t}} = 0.25$ and $r^0_{\mathrm{m:t}} = 5.0$) are mainly made of small oligomers. The distribution of molecular sizes is centered below 200 atoms per molecule. The average number of molecules in the simulation box is large. For $r^0_{\mathrm{m:t}} = 0.25$, the average number of chain ends per molecule is of the order of 2 with almost no TMC monomer fully connected to MPD monomers, meaning chains are almost linear oligomers ending with TMC groups. For $r^0_{\mathrm{m:t}} = 5.0$, the number of chain ends is close to 4 and the total number of monomers is close to 6. This indicates the creation of short chains with 4 MPD terminal groups. The formation of small oligomers is also observed for other $r^0_{\mathrm{m:t}}$ values. Visual inspection of simulation boxes shows that for extreme MPD/TMC ratios, some molecules don't span over the entire box. In such

cases, the system may not behave like a fully connected membrane, as expected in real systems. On the other hand, synthesized systems with intermediate value $r^0_{\mathrm{m:t}} = 1.5$ have a different structure. They contain a smaller number of molecules per box, meaning that polymerization went further than for $r^0_{\mathrm{m:t}} = 0.25$ and $r^0_{\mathrm{m:t}} = 5.0$. The size distribution spreads up to 2000 atoms per molecule. The number of fully cross-linked sites is larger, indicating a more complex molecular shape. Synthesized systems with $r^0_{\mathrm{m:t}}$ values in the range 1.1-1.9 do contain "infinite clusters". This region is roughly indicated on Figs. 6 and 10.

3.4. Chemical structure analysis

In this section, we study the influence of the initial MPD/TMC ratio on the final chemical structure of our samples. Chemical data are presented using oxygen *versus* nitrogen atom plots [61]. Fig. 6 represents such an O/N map obtained from elementary compositions of our samples. The region inside the dashed-red line represents all possible APA compositions (see

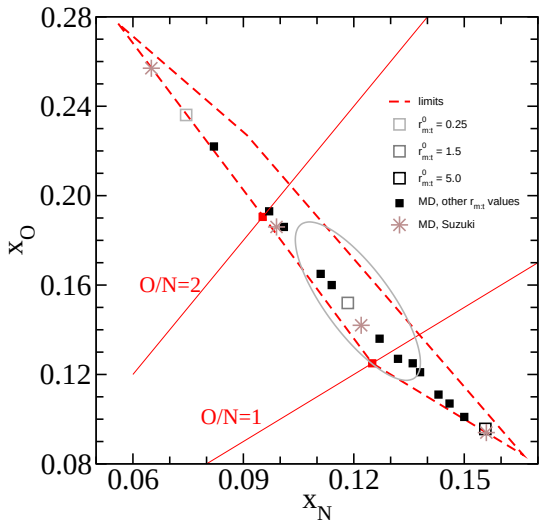

Figure 6: Elemental composition of simulated samples from this work and from Suzuki *et al.* [42]. Data from Suzuki correspond to simulations with $r^0_{\mathrm{m:t}} = 0.25$ (upper left value), 1.0, 1.5 and $r^0_{\mathrm{m:t}} = 4.0$ (lower right value). The region inside the dashed-red lines represents all possible compositions for APA molecules. The region inside the grey ellipse contains simulation boxes with "infinite clusters". The two red square points indicate the O/N coordinates of a fully linear chain ($x_{\mathrm{N}} \approx 0.095$) and a fully cross-linked APA molecule ($x_{\mathrm{N}} \approx 0.125$). The two thin red lines represent O/N ratio of 1 and 2.

Supplementary Information section 1 to see how these limits were obtained). Therefore, any point away from this region may be questionable. The two red square points indicate the O/N coordinates of a fully linear chain ($x_{\mathrm{N}} \approx 0.095$, O/N=2) and a fully cross-linked APA molecule ($x_{\mathrm{N}} \approx 0.125$, O/N=1). Both are hypothetical structures that cannot be found in real systems.

The two red thin lines are values where O/N ratio are equal to 1 and 2, indicating the region where the cross-linking degree is defined ($0 < \chi < 1$ thus from equation 1, we have $1 < \mathrm{O/N} < 2$). Obviously, our simulation data fall inside the dashed red line: The algorithm only allows the formation of APA and the final elemental composition is perfectly known. Statistical error (SE) was computed from the different repetition boxes for $r^0_{\mathrm{m:t}} = 0.25$, 1.5 and 5.0. The SE on composition is smaller than the symbol size (large squares. See Supplementary Information section 2 for SE data). From the upper left point to the lower right point, simulation points correspond to boxes with increasing $r^0_{\mathrm{m:t}}$ value, from 0.25 to 5.0. Along this line, we observe that the oxygen content decreases almost linearly with the nitrogen content. Our data are compared here with the data from Suzuki *et al.* [42]. From upper left to lower right of the graph, their data correspond to simulations with $r^0_{\mathrm{m:t}} = 0.25$, 1.0, 1.5 and 4.0. Considering the random nature of the simulation process, we conclude that the two simulation sets are in good agreement.

Fig. 7 shows O/N maps of our samples on which is superimposed as a color map the value of different descriptors $r_{\mathrm{m:t}}$, χ, f_{ac} and f_{am} computed from elemental composition and equations 1, 4–6. Fig. 7a shows the evolution of the final monomer ratio, $r_{\mathrm{m:t}}$. As $r^0_{\mathrm{m:t}}$ values increase

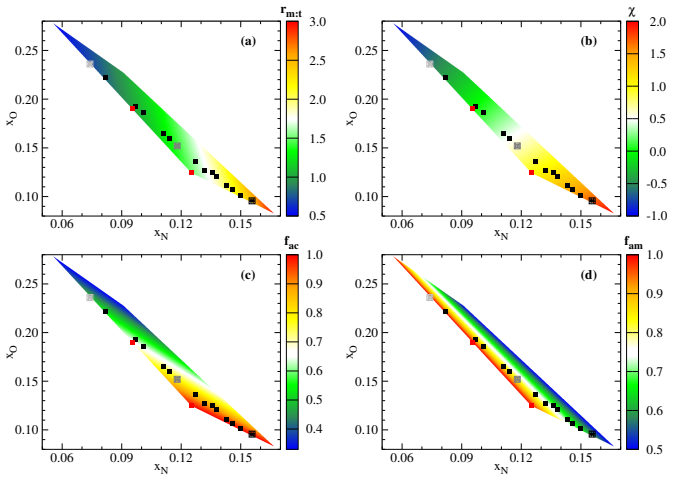

Figure 7: O/N map with chemical structure descriptors $r_{\mathrm{m:t}}$, χ, f_{ac} and f_{am} of simulated APA polymers. The color map is plotted for all possible compositions of APA molecules. The two red square points indicate the O/N coordinates of a fully linear chain ($x_{\mathrm{N}} \approx 0.095$) and a fully cross-linked APA molecule ($x_{\mathrm{N}} \approx 0.125$). Open square and black square symbols: see legend Fig. 6.

from 0.25 to 5.0 with increasing x_{N}, we can see that final MPD/TMC ratio values can be quite different from the initial one, ranging from roughly 0.7 to 2.5. When one type of monomer is present in large excess, many of them do not react leading to a final $r_{\mathrm{m:t}}$ different from $r^0_{\mathrm{m:t}}$, whereas for initial MPD/TMC values in the range $1 < r^0_{\mathrm{m:t}} < 2$ (see Supplementary Information

section 3 for a plot of $r_{\mathrm{m:t}}$ versus $r^0_{\mathrm{m:t}}$), the final $r_{\mathrm{m:t}}$ is closer to the initial one. Thus a better control of the final monomer ratio can be obtained in this $r^0_{\mathrm{m:t}}$ range.

These results compare very well with previous simulation studies. Suzuki *et al.* [42] obtained $r_{\mathrm{m:t}}$ values in the range 0.6-2.5, very close to what is obtained here. Harder *et al.* [27] obtained a single sample with a $r_{\mathrm{m:t}}$ value close to 1. The same group [62] improved their polymerization strategy and obtained a system with a final MPD/TMC ratio equal to 1.1. Wei *et al.* [36] built a large simulation box with a MPD/TMC ratio of 1.32. Globally [27, 23, 63, 25, 26, 34], most authors who prepared a single APA box, obtained membranes with a $r_{\mathrm{m:t}}$ in the range 1.0-1.35, as expected from their initial conditions and polymerization algorithm.

The cross-linking degree χ is shown in Fig. 7b. As mentioned above, this descriptor assumes that APA chains are composed of linear and cross-linked segments only, neglecting the presence of chain ends. Under such assumption, χ must be a positive quantity smaller than 1.

The χ values computed for our systems vary from -0.59 to 1.75 with increasing $r^0_{\mathrm{m:t}}$ (or x_{N} values. See Supplementary Information section 3 for a plot of χ versus $r^0_{\mathrm{m:t}}$). Our samples cover the range of systems previously studied [27, 25, 28] with computed cross-linking degree in the range 0.09–0.83. However, the large range of χ values observed here indicates the presence of a large proportion of chain ends, especially at low or high $r^0_{\mathrm{m:t}}$ values. It also turns out that χ doesn't give a correct qualitative view of the cross-linking degree of the samples. *E.g.*, for system with $r^0_{\mathrm{m:t}} = 0.75$, we have $\chi = 0$ whereas direct inspection of the molecules shows many cross-linked nodes, *i.e.* TMC monomers fully connected with MPD monomers. On the contrary, for system with $r^0_{\mathrm{m:t}} = 2.5$, we have $\chi = 1.2$ but direct inspection of the molecules shows a very limited number of cross-linked nodes. In face of such inconsistency, we consider that the use of the chemical descriptor χ should be done with caution, at least for systems containing a substantial amount of chain ends.

As shown in Fig. 7c and 7d, along with the increase of the initial $r^0_{\mathrm{m:t}}$, the fraction of acyl groups that have reacted f_{ac} increases while that of reacted amine f_{am} decreases (see Supplementary Information section 3 for a plot of f_{ac} and f_{am} versus $r^0_{\mathrm{m:t}}$). For $r^0_{\mathrm{m:t}} < 1$ (*i.e.* TMC is in excess), the fraction of amine groups that have reacted is close to one. The fraction of acyl groups that have reacted is 0.5 or larger. This indicates the formation of molecules with a large amount of TMC like chain ends, *e.g.* $a + 2c$ structure. For $r^0_{\mathrm{m:t}} > 2$, most acyl groups have reacted ($f_{\mathrm{ac}} \to 1$) while molecules exhibit a large number of unreacted amine groups ($f_{\mathrm{am}} \to 0.6$), corresponding to MPD like chain ends ($b+d$ structure). For $1 < r^0_{\mathrm{m:t}} < 2$, relatively

large fractions of acyl and amine have reacted, roughly 80%, indicating a larger efficiency of the polymerization algorithm in this concentration range. For example, the system with $r^0_{\mathrm{m:t}} = 1.8$, which is very close to the fully cross-linked sample on the O/N map, has $r_{\mathrm{m:t}} = 0.96$, $f_{\mathrm{ac}} = 0.85$ and $f_{\mathrm{am}} = 0.79$.

Finally, a great variability is observed for all descriptors, meaning the initial monomer composition has a strong influence onto the final composition obtained through simulated polymerization and different chemical structures have been created. Some structures built in this study have chemical composition close to a fully cross-linked sample, though this ideal structure is never obtained using the simulated polymerization algorithm as presented section 2.2.

3.5. Density

In this section, we present and discuss the density values obtained as a function of the final MPD/TMC ratio. As shown in Fig. 8, a slight decrease of ρ, from 1.29 to 1.23 g/cm^3, is observed with increasing $r_{\mathrm{m:t}}$. However, considering the fact that large structural differences exist between our samples, we can say that the density of APA is almost no sensitive to the details of the chemistry. This behavior is partly confirmed by group contribution estimations. Using data found in van Krevelen book [64], we obtain 1.39 and 1.38 g/cm^3 for the fully linear and fully cross-linked structures respectively (see Supplementary Information section 4 for details). The above discussion suggests that even APA with large amounts of unreacted groups, as seen with extreme values of $r^0_{\mathrm{m:t}}$, have the same density as highly cross-linked systems. This could be attributed to strong hydrogen bonds between hydrogen and oxygen atoms in these free groups to form a structure as dense as a cross-linked network. Short range interactions between aromatic rings (π-π stacking) has also been reported [36], resulting in a dense, thin two-layer slip structure.

Comparison of our data with other simulation results is not easy. Following Kotelyanskii *et al.* [21, 22], many authors built a simulation box based on the experimental density 1.38 g/cm^3 and an estimated water content of the hydrated FT-30 membrane of 23 w% at ambient conditions [27, 23, 62, 24, 19, 25, 26, 42]. After a short relaxation time, an hydrated density in the range 1.30–1.39 g/cm^3, corresponding to a dry density in the range 1.0–1.1 g/cm^3 is obtained. These dry density values must be taken with caution as they were obtained after relaxation times much shorter than the one used here and, most importantly, they correspond to the density of a swollen polymer. Kolev and Freger [28] computed, using molecular simulation, the density of

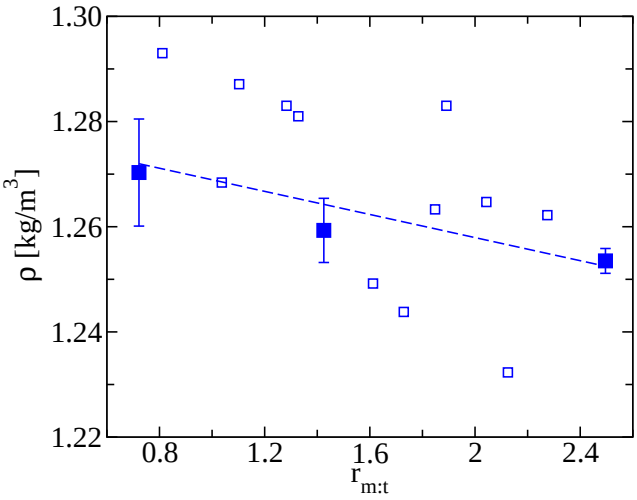

Figure 8: Density versus $r_{\mathrm{m:t}}$ for sample equilibrated in the iso-stress ensemble. Large square symbols represent the average density for the 11 repetition boxes at respective $r_{\mathrm{m:t}}$. The dashed-line is a linear regression over all data and accounts for the different statistical weight of each data point.

the same hydrated (hence swollen) and dry membrane and showed that the calculated density increases by about 10%. A density value of 1.24 g/cm^3 including large voids is proposed while an average density of the dense region is about 1.3 g/cm^3 for the dry polymer. This range is in full agreement with our set samples. Recent available data for other models of unswollen dry membrane densities [29, 36, 30, 33] lie in the range 1.17-1.31 g/cm^3. Finally we can conclude that recent molecular simulation values are in good agreement with the average computed from the 11 repetition boxes at $r^0_{\mathrm{m:t}} = 1.5$ where $\rho = 1.26 \pm 0.02$ g/cm^3.

4. Discussion: simulated versus real membrane properties

In this section, we try to relate our simulation results to experimental data on APA RO membrane layer. It is important to keep in mind that molecular simulations, because of time and length scale limitations, propose a model of the dense region of the APA membrane.

The density of the membrane is a typical macroscopic quantity whose knowledge is important for many transfer and partitioning predictive models. However, the experimental determination of the dry density of the dense region in the membrane is a difficult task because of the complex morphology of APA layers. Zhang *et al.* [41] used water adsorption experiments with quartz microbalance to determine water uptake for the FT30 and LF10 reverse osmosis membranes

and obtained values of 11.2 w/w% and 12.8 w/w% respectively. Using the experimental density value of 1.38 g/cm^3 given in [21], they deduced a FT30 active layer density of 1.24 g/cm^3 and a LF10 active layer density of 1.22 g/cm^3. Lin *et al.* [65] measured dry densities of several APA layers from reverse osmosis and nano-filtration membranes. The volumetric density is computed as the areal mass of active layer measured using quartz microbalance divided by the thickness obtained by ellipsometry analyses; it averages to 1.26 ± 0.21 g/cm^3 for the uncoated APA active layers. However, these studies do not compute the density of the dense region of the APA active layer but rather an effective dry density including existing voids. Very recently, we measured the density of the APA layer of the reverse osmosis CPA2 commercial membrane [60]. The study was based on the measurement of the effective surface density, the membrane thickness and the void fraction. Density values of 1.18±0.14 g/cm^3 and 1.30±0.14 g/cm^3 were obtained using AFM and profilometry thickness analysis respectively, leading to an average value of 1.24 g/cm^3 for the dense region of CPA2 active layer membrane. Therefore, the good agreement between our simulation results and the experimentally determined density of the dense region [60] validates the force field and the general procedure used here. Moreover, molecular simulations show that the mass density of APA membranes does not depend on the details of their chemistry.

The separation performances of active layer of reverse osmosis membranes is controlled by water permeability and solute selectivity. It is widely accepted that free volume holes between cross-linked polymer chains play an important role in small molecules transfer. Positron annihilation lifetime spectroscopy (PALS) is an analytical technique using positron annihilation spectroscopy (PAS) which allows for the measurement of the mean size of subnanometre-scale holes (*i.e.* free volume hole-size). This technique has been employed by several authors in the context of reverse osmosis membranes characterization. Henmi *et al.* [66] evaluated boron rejection using similar types of membranes and reported that the rejection of boron decreased with increasing free volume. Chen *et al.* [67] reported that the rejection of four neutral solutes (urea, ethylene, 1-propanol, and 2-propanol) correlated well with the ratio of the molecular volume of solutes to the volume of sphere-shaped free volume holes in the membrane. Fujioka *et al.* [68] reviewed data obtained for RO membranes and suggest to include other techniques *e.g.* molecular dynamics simulations to describe the internal structure of APA membranes. We computed the fraction of accessible volume (FAV) defined as the volume occupied by hard-spheres with van der Waals radius divided by the box volume [69] (see Supplementary Information section 5 for more details on the methodology employed). Generally speaking, the free volume depends

on chain rigidity and the proportion of chain ends (which tends to increase the free volume). In the case of APA, we believe that the presence of short cross-links between linear segments leave some empty space that could not be filled by the polymer because of chain rigidity. As can be seen in Fig. 9, the general trend is that the FAV slightly decreases with $r_{\mathrm{m:t}}$ (or $r^0_{\mathrm{m:t}}$). It is accompanied by an increase of the proportion of the chain ends density N^t_{ce}/V (N^t_{ce} is the total number of chain ends in the simulation box, V is the simulation box volume), mostly seen for $r_{\mathrm{m:t}}$ larger than one. The increase of the density of cross-linked TMC units N^t_{cl}/V (N^t_{cl} is the

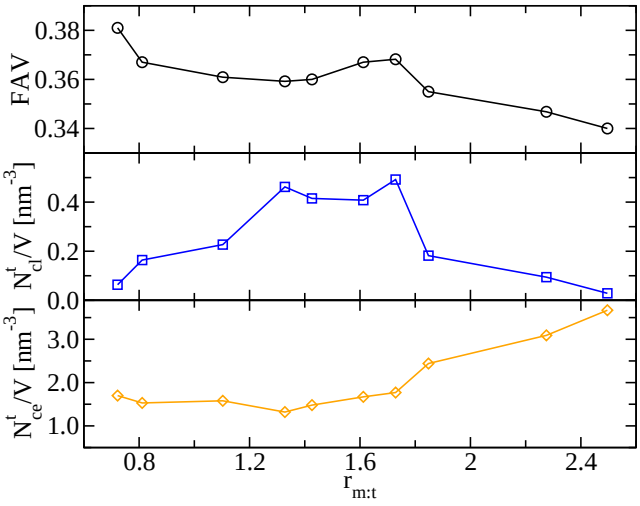

Figure 9: Evolution of the free accessible volume (FAV), the number of cross-linked points per unit volume (N^t_{cl}/V) and the number of chain ends per unit volume (N^t_{ce}/V) with $r_{\mathrm{m:t}}$.

total number of cross-linked TMC units), seen for $1.3 < r_{\mathrm{m:t}} < 1.7$, seems to be associated with an increase of the FAV. Unfortunately, because of poor statistics, we were not able to establish a clear link between FAV and the concentration of chain ends and cross-linking point densities in our samples. Nonetheless, it would be interesting to establish such a correlation in order to tailor membrane properties from proportion of chain end and cross-linking points.

From a microscopic point of view, our simulations reveal that the fraction of reacted amine and acyl groups varies in a large range. It is clear that most of the systems studied at high excess of MPD or TMC monomers lead to unrealistic polymers. Meanwhile, boxes with initial MPD/TMC ratio in the range 1–2 provide systems with composition compatible with almost fully linear samples and highly cross-linked samples. For these systems, a non negligible amount of unreacted amine and carboxylic acid groups is found. Signature for these groups have already been mentioned in the literature. Using tangential streaming ζ-potential measurements [70] it is possible to determine surface charges at the interface between various reverse osmosis mem-

branes and an electrolyte. Due to their composition, uncoated membranes can have a positive charge at acidic pH because of the ionization of the free amine groups at their surface into $–NH_3^+$. When pH rises, the ζ-potential becomes negative because of the dissociation of free carboxylic groups of TMC into COO^- and the neutralization of NH_3^+ groups.

Infrared spectroscopy is extensively used to check presence of coating on commercial membranes. Though, a few studies used IR to reveal the presence of carboxylic and amine groups. Dutta *et al.* [16] mention that for membranes synthesized using reacting solutions of 1% TMC and 8% MPD, an excess of amine groups in the sample is observable in FTIR spectra, with an enhancement of the band at 1666–1670 cm^{-1}. Identically, for polymers synthesized using 1% TMC and 2% MPD concentration solutions, they noticed –OH stretching frequency bands at 3751 and 3856 cm^{-1}. A relatively weak band is also observed by Mi *et al.* [71] at 1450 cm^{-1} corresponding to the presence of carboxylic acid groups. Jin *et al.* [72] assigned the vibrational band at 1720 cm^{-1} to the C=O stretching of carboxylic acid groups for layers synthesized with 4 wt/v% MPD solution and 0.5 to 2 wt/v% TMC solutions. Using spectrum bands deconvolution, they were able to observe the increase in COOH groups with increasing TMC solution concentration. We computed IR spectra from molecular simulation trajectories of our samples to compare with existing data in the literature. Although a clear evolution is seen for several bands indicating concentration changes of amine, carboxylic and amide groups, the results are barely comparable with experiments (see Supplementary Information section 6 and figures therein). Absorption bands specific of amide groups [61] (1660, 1610 and 1540 cm^{-1} corresponding to C=O signal *amide I*, aromatic ring breathing and C-N stretching *amide II*) appear at different frequencies than experimental one, due to intramolecular force field and methodological limitations. Group concentrations could be deduced from the computed IR spectra in the high frequency range (3000-4000 cm^{-1}) but unfortunately, this doesn't seem to be applicable to real spectra where the resolution is much lower in this frequency range.

It is widely accepted that the active layer structure is chemically heterogeneous throughout its depth [73, 74, 75, 76]. Wamser and Gilbert [73] concluded from contact angle titration experiments that carboxylic and amine groups predominate at the APA top-surface (TS) and back-surface (BS) respectively. Freger [75] demonstrated that the polymer charge is distributed across the active polyamide layer in a highly non uniform fashion. The polyamide films appear to be built of a negatively charged outer layer (carboxylic-rich region) sitting on top of an

inner layer possessing a small positive charge (amine-rich region). Using X-ray photoelectron spectrometry (XPS) and Rutherford backscattering spectrometry (RBS), Coronell *et al.* [76] extensive analysis of reverse osmosis and nano filtration membranes, support the existence of both depth-homogeneous and depth-heterogeneous active layers. Such studies indicate that in order to improve the current understanding of permeation phenomena during reverse osmosis filtration, there is a need to characterize as a function of depth the physicochemical properties and interactions with contaminants inside active layers.

Fig. 10 presents oxygen versus nitrogen atom fraction map and compares chemical composition between our simulation data and conventional reverse osmosis membranes. Six sets of experimental data are presented: Song *et al.* [60] data where the APA layer of the commercial membrane CPA2 has been studied using XPS analysis on top-surface and back-surface (after removal of the support layer); results from Coronell *et al.* [76] on three different reverse osmosis membranes analyzed using XPS (for the top-surface) and RBS to get insights into chemical heterogeneities along the thickness of the APA layer; data from Park *et al.* [77] using XPS analysis on supported and support-free synthesized APA membranes and where the back-surface (APA membrane surface in contact with the aqueous phase during the polymerization) was analyzed for the support-free polymerized membrane; XPS data from Park *et al.* [78] for APA membranes synthesized on PSf and hybrid metal organic framework/PSf support; a selection of Tang *et al.* [61] XPS data for polyamide thin films of 6 commonly used commercial RO membranes; Xu *et al.* [18] XPS analysis of various APA layers prepared by changing the monomer concentrations in a wide range.

Experimental data are presented according to three different criteria: top-surface data (TS, upper triangles) and back-surface data (BS, lower triangles), both obtained using XPS measurements and data obtained using RBS experiments, giving an average elemental composition of the layer.

We first notice that experimental data are rather scattered over the O/N map and many points fall out of the limits imposed by the stoichiometry of APA polymers. This is particularly true for XPS analyses. It may well be that surface contamination by chemicals alter the final composition. However, this figure demonstrates the influence of the synthesis parameters onto the final composition. One can also notice that top-surfaces (triangle up) generally have smaller nitrogen content than the average composition (square) and the highest nitrogen values correspond to data obtained on back-surface (triangle down). This is in agreement with the general

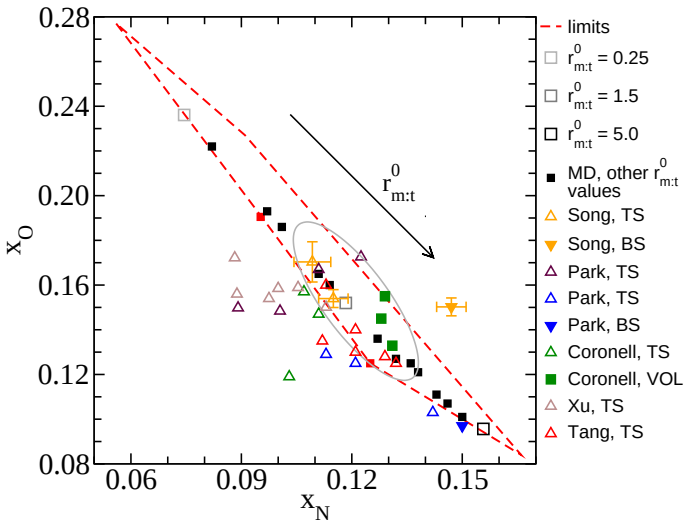

Figure 10: Elemental composition of simulated samples and several commercial and home-made APA reverse osmosis membrane layers. Squares represent data corresponding to an average composition (molecular simulations or RBS experiments). Upper and lower triangles represent XPS data from top-surface (TS) and back-surface (BS) analyses of the membranes, respectively. Colors refer to different works or publications; black: molecular simulations, this work; orange: Song *et al.* [60]; blue: Park *et al.* [77]; maroon: Park *et al.* [78]; green: Coronell *et al.* [76]; brown: Xu *et al.* [18]; red: Tang *et al.* [61]. The region inside the dashed-red lines represents all possible compositions for APA molecules. The region inside the grey ellipse contains simulation boxes with "infinite clusters".

result obtained by Wamser [73] or Freger [75] that carboxylic and amine groups predominate at the APA top-surface and back-surface respectively, because during membrane synthesis the local MPD concentration decreases from the aqueous-organic interface to the pure organic phase. The interesting point is that our simulation data are in agreement with this behavior. As the initial MPD/TMC ratio is increased, final nitrogen content increases and our samples share characteristics with back-surface region. Inversely, when the initial MPD/TMC ratio decreases, final nitrogen content decreases and the simulation boxes resemble membrane top-surface region. The different simulation boxes could thus be used to describe a particular region of the membrane, from the back-surface, to the top-surface.

5. Conclusions

Molecular simulation has been used to build APA polymer samples. Our aim was to study how local monomer composition that appear during interfacial polymerization affect the structure of a model of APA membrane. We covered a rather large range of initial MPD/TMC monomer ratios, from 1:4 to 5:1, and did observe many different structures. The polymerization step in

itself requires short simulation times but full strains relaxation required up to several microseconds.

For systems with large excess of TMC or MPD monomers, the behavior is almost "pathological" with the formation a small oligomers with linear structure and few reticulation nodes. The fraction of unreacted acyl and amine groups is high for $r^0_{\mathrm{m:t}} \to 0.25$ and $r^0_{\mathrm{m:t}} \to 5.0$ respectively. For $1 < r_{\mathrm{m:t}} < 2$, synthesized samples have chemical composition typical of APA membranes ($0.09 < x_{\mathrm{N}} < 0.13$ and $0.12 < x_{\mathrm{O}} < 0.18$). The fraction of acyl and amine groups that have reacted is high although different from 1, indicating that numerous chain ends still exist in these structures. It is likely that during the polymerization steps, amine or acyl groups are trapped inside the chemical structure and are no longer accessible to other reactants, being large oligomers or even a single monomer.

We believe that the simulated samples created under different local concentrations can describe properly the chemical heterogeneities observed experimentally in reverse osmosis membranes. We think that the methodology employed is a tool to produce membranes with slightly different chemical compositions and to investigate their selectivity performances. As mentioned by Freger and Ramon in a recent review [79], experimentally determined parameters such as density or cross-linking degree may not reflect the film behavior as a selective membrane. This study contributed to the preparation, at the molecular level, of samples with different structural characteristics. We belive that further molecular simulation studies to investigate their selectivity performances, could provide better insights into the structure-property relationships.

Funding sources

This study was partially supported (X.S. PhD grant) by the Doctoral School "Agriculture, alimentation, biologie, environnement et santé (ABIES)" through finances from AgroParisTech, Université Paris-Saclay, grant number 2017-3.

Appendix A. Supplementary information

Detailed information on the definition of compositional limits for APA polymers, statistic errors from repetition boxes, descriptor evolution with $r^0_{\mathrm{m:t}}$, density computed using group contribution method, fractional accessible free volume computations and infrared spectrum computation is presented in the supplementary information.

References

[1] N. M. Al-Bastaki, Performance of advanced methods for treatment of wastewater: UV/TiO2, RO and UF, Chem. Eng. Process.: Proc. Intensif. 43 (7) (2004) 935–940. doi:10.1016/j.cep.2003.08.003.

[2] A. Sonune, R. Ghate, Developments in wastewater treatment methods, Desalination 167 (2004) 55–63. doi:10.1016/j.desal.2004.06.113.

[3] S. S. Shenvi, A. M. Isloor, A. Ismail, A review on RO membrane technology: Developments and challenges, Desalination 368 (2015) 10–26. doi:10.1016/j.desal.2014.12.042.

[4] I. Frenzel, D. F. Stamatialis, M. Wessling, Water recycling from mixed chromic acid waste effluents by membrane technology, Sep. Purif. Technol. 49 (1) (2006) 76–83. doi:10.1016/j.seppur.2005.08.010.

[5] J. Hoinkis, V. Panten, Wastewater recycling in laundries—from pilot to large-scale plant, Chem. Eng. Process.: Proc. Intensif. 47 (7) (2008) 1159–1164. doi:10.1016/j.cep.2007.12.010.

[6] C. Sagne, C. Fargues, R. Lewandowski, M.-L. Lameloise, M. Gavach, M. Decloux, A pilot scale study of reverse osmosis for the purification of condensate arising from distillery stillage concentration plant, Chem. Eng. Process.: Proc. Intensif. 49 (4) (2010) 331–339. doi:10.1016/j.cep.2010.03.002.

[7] C. Li, Y. Yang, Y. Liu, L.-a. Hou, Removal of PhACs and their impacts on membrane fouling in NF/RO membrane filtration of various matrices, J. Membr. Sci. 548 (2018) 439–448. doi:10.1016/j.memsci.2017.11.032.

[8] K. Licona, L. d. O. Geaquinto, J. Nicolini, N. Figueiredo, S. Chiapetta, A. Habert, L. Yokoyama, Assessing potential of nanofiltration and reverse osmosis for removal of toxic pharmaceuticals from water, J. Water Proc. Eng. 25 (2018) 195–204. doi:10.1016/j.jwpe.2018.08.002.

[9] K. V. Plakas, A. J. Karabelas, Removal of pesticides from water by NF and RO membranes — a review, Desalination 287 (2012) 255–265. doi:10.1016/j.desal.2011.08.003.

[10] H. T. Madsen, E. G. Søgaard, Applicability and modelling of nanofiltration and reverse osmosis for remediation of groundwater polluted with pesticides and pesticide transformation products, Sep. Purif. Technol. 125 (2014) 111–119. doi:10.1016/j.seppur.2014.01.038.

[11] R. Mehta, H. Brahmbhatt, N. Saha, A. Bhattacharya, Removal of substituted phenyl urea pesticides by reverse osmosis membranes: Laboratory scale study for field water application, Desalination 358 (2015) 69–75. doi:10.1016/j.desal.2014.12.019.

[12] M. Nikbakht Fini, H. T. Madsen, J. Muff, The effect of water matrix, feed concentration and recovery on the rejection of pesticides using NF/RO membranes in water treatment, Sep. Purif. Technol. 215 (2019) 521–527. doi:10.1016/j.seppur.2019.01.047.

[13] J. E. Cadotte, R. J. Petersen, R. E. Larson, E. E. Erickson, A new thin-film composite seawater reverse osmosis membrane, Desalination 32 (C) (1980) 25–31. doi:10.1016/S0011-9164(00)86003-8.

[14] S. Habib, S. T. Weinman, A review on the synthesis of fully aromatic polyamide reverse osmosis membranes, Desalination 502 (2021) 114939. doi:10.1016/j.desal.2021.114939.

[15] G.-Y. Chai, W. B. Krantz, Formation and characterization of polyamide membranes via interfacial polymerization, J. Membr. Sci. 93 (2) (1994) 175–192. doi:10.1016/0376-7388(94)80006-5.

[16] D. Dutta, A. Bhattacharyya, B. Ganguly, Microstructural study of aromatic polyamide membrane material, J. Membr. Sci. 224 (1-2) (2003) 127–135. doi:10.1016/j.memsci.2003.08.001.

[17] B. Khorshidi, T. Thundat, B. A. Fleck, M. Sadrzadeh, A novel approach toward fabrication of high performance thin film composite polyamide membranes, Sci. Rep. 6 (1) (2016) 22069. doi:10.1038/srep22069.

[18] J. Xu, H. Yan, Y. Zhang, G. Pan, Y. Liu, The morphology of fully-aromatic polyamide separation layer and its relationship with separation performance of TFC membranes, J. Membr. Sci. 541 (2017) 174–188. doi:10.1016/j.memsci.2017.06.057.

[19] H. Ebro, Y. M. Kim, J. H. Kim, Molecular dynamics simulations in membrane-based water treatment processes: A systematic overview, J. Membr. Sci. 438 (2013) 112–125. doi:10.1016/j.memsci.2013.03.027.

[20] H. F. Ridgway, J. Orbell, S. Gray, Molecular simulations of polyamide membrane materials used in desalination and water reuse applications: Recent developments and future prospects, J. Membr. Sci. 524 (October 2016) (2017) 436–448. doi:10.1016/j.memsci.2016.11.061.

[21] M. J. Kotelyanskii, N. J. Wagner, M. E. Paulaitis, Atomistic simulation of water and salt transport in the reverse osmosis membrane FT-30, J. Membr. Sci. 139 (1) (1998) 1–16. doi:10.1016/S0376-7388(97)00220-2.

[22] M. J. Kotelyanskii, N. J. Wagner, M. E. Paulaitis, Molecular dynamics simulation study of the mechanisms of water diffusion in a hydrated, amorphous polyamide, Comput. Theor. Polym. Sci. 9 (3-4) (1999) 301–306. doi:10.1016/S1089-3156(99)00020-3.

[23] Z. E. Hughes, J. D. Gale, A computational investigation of the properties of a reverse osmosis membrane, J. Mater. Chem. 20 (36) (2010) 7788–7799. doi:10.1039/c0jm01545h.

[24] Z. E. Hughes, J. D. Gale, Molecular dynamics simulations of the interactions of potential foulant molecules and a reverse osmosis membrane, J. Mater. Chem. 22 (1) (2012) 175–184. doi:10.1039/C1JM13230J.

[25] Y. Xiang, Y. Liu, B. Mi, Y. Leng, Hydrated polyamide membrane and its interaction with alginate: A molecular dynamics study, Langmuir 29 (37) (2013) 11600–11608. doi:10.1021/la401442r.

[26] M. Ding, A. Ghoufi, A. Szymczyk, Molecular simulations of polyamide reverse osmosis membranes, Desalination 343 (2014) 48–53. doi:10.1016/j.desal.2013.09.024.

[27] E. Harder, D. E. Walters, Y. D. Bodnar, R. S. Faibish, B. Roux, Molecular dynamics study of a polymeric reverse osmosis membrane, J. Phys. Chem. B 113 (30) (2009) 10177–10182. doi:10.1021/jp902715f.

[28] V. Kolev, V. Freger, Hydration, porosity and water dynamics in the polyamide layer of reverse osmosis membranes: A molecular dynamics study, Polymer 55 (6) (2014) 1420–1426. doi:10.1016/j.polymer.2013.12.045.

[29] M. Shen, S. Keten, R. M. Lueptow, Dynamics of water and solute transport in polymeric reverse osmosis membranes via molecular dynamics simulations, J. Membr. Sci. 506 (2016) 95–108. doi:10.1016/j.memsci.2016.01.051.

[30] T. P. Liyana-Arachchi, J. F. Sturnfield, C. M. Colina, Ultrathin molecular-layer-by-layer polyamide membranes: Insights from atomistic molecular simulations, J. Phys. Chem. B 120 (35) (2016) 9484–9494. doi:10.1021/acs.jpcb.6b02801.

[31] R. Nadler, S. Srebnik, Molecular simulation of polyamide synthesis by interfacial polymerization, J. Membr. Sci. 315 (1-2) (2008) 100–105. doi:10.1016/j.memsci.2008.02.023.

[32] R. Oizerovich-Honig, V. Raim, S. Srebnik, Simulation of thin film membranes formed by interfacial polymerization, Langmuir 26 (1) (2010) 299–306. doi:10.1021/la9024684.

[33] J. Muscatello, E. Müller, A. Mostofi, A. Sutton, Multiscale molecular simulations of the formation and structure of polyamide membranes created by interfacial polymerization, J. Membr. Sci. 527 (2017) 180–190. doi:10.1016/j.memsci.2016.11.024.

[34] M. Ding, A. Szymczyk, F. Goujon, A. Soldera, A. Ghoufi, Structure and dynamics of water confined in a polyamide reverse-osmosis membrane: A molecular-simulation study, J. Membr. Sci. 458 (2014) 236–244. doi:10.1016/j.memsci.2014.01.054.

[35] M. Ding, A. Szymczyk, A. Ghoufi, On the structure and rejection of ions by a polyamide membrane in pressure-driven molecular dynamics simulations, Desalination 368 (2015) 76–80. doi:10.1016/j.desal.2015.01.003.

[36] T. Wei, L. Zhang, H. Zhao, H. Ma, M. S. J. Sajib, H. Jiang, S. Murad, Aromatic polyamide reverse-osmosis membrane: An atomistic molecular dynamics simulation, J. Phys. Chem. B 120 (39) (2016) 10311–10318. doi:10.1021/acs.jpcb.6b06560.

[37] A. Ghoufi, E. Dražević, A. Szymczyk, Interactions of organics within hydrated selective layer of reverse osmosis desalination membrane: A combined experimental and computational study, Environ. Sci. Technol. 51 (5) (2017) 2714–2719. doi:10.1021/acs.est.6b05153.

[38] L. Yao, Z. Qin, Q. Chen, M. Zhao, H. Zhao, W. Ahmad, L. Fan, L. Zhao, Insights into the nanofiltration separation mechanism of monosaccharides by molecular dynamics simulation, Sep. Purif. Technol. 205 (2018) 48–57. doi:10.1016/j.seppur.2018.04.056.

[39] Y.-l. Liu, X.-m. Wang, H.-w. Yang, Y. F. Xie, Quantifying the influence of solute-membrane interactions on adsorption and rejection of pharmaceuticals by NF/RO membranes, J. Membr. Sci. 551 (2018) 37–46. doi:10.1016/j.memsci.2018.01.035.

[40] Y.-l. Liu, K. Xiao, A.-q. Zhang, X.-m. Wang, H.-w. Yang, X. Huang, Y. F. Xie, Exploring the interactions of organic micropollutants with polyamide nanofiltration membranes: A molecular docking study, J. Membr. Sci. 577 (2019) 285–293. doi:10.1016/j.memsci.2019.02.017.

[41] X. Zhang, D. G. Cahill, O. Coronell, B. J. Mariñas, Absorption of water in the active layer of reverse osmosis membranes, J. Membr. Sci. 331 (1-2) (2009) 143–151. doi:10.1016/j.memsci.2009.01.027.

[42] Y. Suzuki, Y. Koyano, M. Nagaoka, Influence of monomer mixing ratio on membrane nanostructure in interfacial polycondensation: Application of hybrid MC/MD reaction method with minimum bond convention, J. Phys. Chem. B 119 (22) (2015) 6776–6785. doi:10.1021/jp512333h.

[43] P. Dauber-Osguthorpe, V. A. Roberts, D. J. Osguthorpe, J. Wolff, M. Genest, A. T. Hagler, Structure and energetics of ligand binding to proteins:escherichia coli dihydrofolate reductase-trimethoprim, a drug-receptor system, Proteins: Struct., Funct., Genet. 4 (1) (1988) 31–47. doi:10.1002/prot.340040106.

[44] A. D. MacKerell, D. Bashford, M. Bellott, R. L. Dunbrack, J. D. Evanseck, M. J. Field, S. Fischer, J. Gao, H. Guo, S. Ha, D. Joseph-McCarthy, L. Kuchnir, K. Kuczera, F. T. K. Lau, C. Mattos, S. Michnick, T. Ngo, D. T. Nguyen, B. Prodhom, W. E. Reiher, B. Roux, M. Schlenkrich, J. C. Smith, R. Stote, J. Straub, M. Watanabe, J. Wiórkiewicz-Kuczera, D. Yin, M. Karplus, All-atom empirical potential for molecular modeling and dynamics studies of proteins †, J. Phys. Chem. B 102 (18) (1998) 3586–3616. doi:10.1021/jp973084f.

[45] J. W. Ponder, D. A. Case, Force fields for protein simulations, in: Advances in Protein Chemistry, Vol. 66, Elsevier, 2003, pp. 27–85. doi:10.1016/S0065-3233(03)66002-X.

[46] J. Wang, R. M. Wolf, J. W. Caldwell, P. A. Kollman, D. A. Case, Development and testing of a general amber force field, J. Comput. Chem. 25 (9) (2004) 1157–1174. doi:10.1002/jcc.20035.

[47] W. L. Jorgensen, D. S. Maxwell, J. Tirado-Rives, Development and testing of the OPLS all-atom force field on conformational energetics and properties of organic liquids, J. Am. Chem. Soc. 118 (45) (1996) 11225–11236. doi:10.1021/ja9621760.

[48] B. L. Eggimann, A. J. Sunnarborg, H. D. Stern, A. P. Bliss, J. I. Siepmann, An online parameter and property database for the TraPPE force field, Mol. Simul. 40 (1-3) (2014) 101–105. doi:10.1080/08927022.2013.842994.

[49] W. L. Jorgensen, J. Chandrasekhar, J. D. Madura, R. W. Impey, M. L. Klein, Comparison of simple potential functions for simulating liquid water, J. Chem. Phys. 79 (2) (1983) 926–935. doi:10.1063/1.445869.

[50] J. L. F. Abascal, C. Vega, A general purpose model for the condensed phases of water: TIP4P/2005, J. Chem. Phys. 123 (23) (2005) 234505. doi:10.1063/1.2121687.

[51] S. Plimpton, Fast parallel algorithms for short-range molecular dynamics, J. Comput. Phys. 117 (1) (1995) 1–19. doi:10.1006/jcph.1995.1039.

[52] LAMMPS molecular dynamics simulator, http://lammps.sandia.gov.

[53] N.-T. Van-Oanh, C. Houriez, B. Rousseau, Viscosity of the 1-ethyl-3-methylimidazolium bis(trifluoromethylsulfonyl)imide ionic liquid from equilibrium and nonequilibrium molecular dynamics, Phys. Chem. Chem. Phys. 12 (4) (2010) 930–936. doi:10.1039/B918191A.

[54] R. W. Hockney, J. W. Eastwood, Computer Simulation Using Particles, IOP Publishing Ltd, 1988. doi:10.1887/0852743920.

[55] W. Shinoda, M. Shiga, M. Mikami, Rapid estimation of elastic constants by molecular dynamics simulation under constant stress, Phys. Rev. B: Condens. Matter Mater. Phys. 69 (13) (2004) 16–18. doi:10.1103/PhysRevB.69.134103.

[56] O. Coronell, B. J. Mariñas, X. Zhang, D. G. Cahill, Quantification of functional groups and modeling of their ionization behavior in the active layer of FT30 reverse osmosis membrane, Environ. Sci. Technol. 42 (14) (2008) 5260–5266. doi:10.1021/es8002712.

[57] O. Coronell, M. I. González, B. J. Mariñas, D. G. Cahill, Ionization behavior, stoichiometry of association, and accessibility of functional groups in the active layers of reverse osmosis and nanofiltration membranes, Environ. Sci. Technol. 44 (17) (2010) 6808–6814. doi:10.1021/es100891r.

[58] X. Song, Structural characterization and molecular modeling of the active aromatic polyamide layer in reverse-osmosis membranes, Ph.D. thesis, Université Paris Saclay (2020).

[59] J. M. Dennison, X. Xie, C. J. Murphy, D. G. Cahill, Density, elastic constants, and thermal conductivity of interfacially polymerized polyamide films for reverse osmosis membranes, ACS Appl. Nano Mater. 1 (9) (2018) 5008–5018. doi:10.1021/acsanm.8b01129.

[60] X. Song, W. Guiga, B. Rousseau, A. Jonquieres, R. Weil, M. Grzelka, J. Waeytens, A. Dazzi, D. Dragoe, C. Fargues, Experimental characterization of commercial and synthesized aromatic polyamide films for reverse osmosis membranes, Ind. Eng. Chem. Res. 60 (7) (2021) 2898–2910. doi:10.1021/acs.iecr.0c05393.

[61] C. Y. Tang, Y.-N. Kwon, J. O. Leckie, Effect of membrane chemistry and coating layer on physiochemical properties of thin film composite polyamide RO and NF membranes, Desalination 242 (1-3) (2009) 149–167. doi:10.1016/j.desal.2008.04.003.

[62] Y. Luo, E. Harder, R. S. Faibish, B. Roux, Computer simulations of water flux and salt permeability of the reverse osmosis FT-30 aromatic polyamide membrane, J. Membr. Sci. 384 (1-2) (2011) 1–9. doi:10.1016/j.memsci.2011.08.057.

[63] Y. Luo, B. Roux, Simulation of osmotic pressure in concentrated aqueous salt solutions, J. Phys. Chem. Lett. 1 (1) (2010) 183–189. doi:10.1021/jz900079w.

[64] D. W. van Krevelen, K. te Nijenhuis, Properties of Polymers: Their Correlation with Chemical Structure: Their Numerical Estimation and Prediction from Additive Group Contributions, 4th Edition, Elsevier, Amsterdam, 2009.

[65] L. Lin, C. Feng, R. Lopez, O. Coronell, Identifying facile and accurate methods to measure the thickness of the active layers of thin-film composite membranes – A comparison of seven characterization techniques, J. Membr. Sci. 498 (2016) 167–179. doi:10.1016/j.memsci.2015.09.059.

[66] M. Henmi, Y. Fusaoka, H. Tomioka, M. Kurihara, High performance RO membranes for desalination and wastewater reclamation and their operation results, Water Sci. Technol. 62 (9) (2010) 2134–2140. doi:10.2166/wst.2010.396.

[67] Z. Chen, K. Ito, H. Yanagishita, N. Oshima, R. Suzuki, Y. Kobayashi, Correlation study between free-volume holes and molecular separations of composite membranes for reverse osmosis processes by means of variable-energy positron annihilation techniques, J. Phys. Chem. C 115 (37) (2011) 18055–18060. doi:10.1021/jp203888m.

[68] T. Fujioka, N. Oshima, R. Suzuki, W. E. Price, L. D. Nghiem, Probing the internal structure of reverse osmosis membranes by positron annihilation spectroscopy: Gaining more insight into the transport of water and small solutes, J. Membr. Sci. 486 (2015) 106–118. doi:10.1016/j.memsci.2015.02.007.

[69] D. Hofmann, M. Entrialgo-Castano, A. Lerbret, M. Heuchel, Y. Yampolskii, Molecular modeling investigation of free volume distributions in stiff chain polymers with conventional and ultrahigh free volume: Comparison between molecular modeling and positron lifetime studies, Macromolecules 36 (22) (2003) 8528–8538. doi:10.1021/ma034971l.

[70] C. Fargues, C. Sagne, A. Szymczyk, P. Fievet, M. L. Lameloise, Adsorption of small organic solutes from beet distillery condensates on reverse-osmosis membranes: Consequences on the process performances, J. Membr. Sci. 446 (2013) 132–144. doi:10.1016/j.memsci.2013.05.051.

[71] B. Mi, D. G. Cahill, B. J. Mariñas, Physico-chemical integrity of nanofiltration/reverse osmosis membranes during characterization by rutherford backscattering spectrometry, J. Membr. Sci. 291 (1-2) (2007) 77–85. doi:10.1016/j.memsci.2006.12.052.

[72] Y. Jin, Z. Su, Effects of polymerization conditions on hydrophilic groups in aromatic polyamide thin films, J. Membr. Sci. 330 (1-2) (2009) 175–179. doi:10.1016/j.memsci.2008.12.055.

[73] C. C. Wamser, M. I. Gilbert, Detection of surface functional group asymmetry in interfacially-polymerized films by contact angle titrations, Langmuir 8 (6) (1992) 1608–1614. doi:10.1021/la00042a019.

[74] V. Freger, S. Srebnik, Mathematical model of charge and density distributions in interfacial polymerization of thin films, J. Appl. Polym. Sci. 88 (5) (2003) 1162–1169. doi:10.1002/app.11716.

[75] V. Freger, Nanoscale heterogeneity of polyamide membranes formed by interfacial polymerization, Langmuir 19 (11) (2003) 4791–4797. doi:10.1021/la020920q.

[76] O. Coronell, B. J. Mariñas, D. G. Cahill, Depth heterogeneity of fully aromatic polyamide active layers in reverse osmosis and nanofiltration membranes, Environ. Sci. Technol. 45 (10) (2011) 4513–4520. doi:10.1021/es200007h.

[77] S. J. Park, W. Choi, S. E. Nam, S. Hong, J. S. Lee, J. H. Lee, Fabrication of polyamide thin film composite reverse osmosis membranes via support-free interfacial polymerization, J. Membr. Sci. 526 (2017) 52–59. doi:10.1016/j.memsci.2016.12.027.

[78] H. M. Park, K. Y. Jee, Y. T. Lee, Preparation and characterization of a thin-film composite reverse osmosis membrane using a polysulfone membrane including metal-organic frameworks, J. Membr. Sci. 541 (2017) 510–518. doi:10.1016/j.memsci.2017.07.034.

[79] V. Freger, G. Z. Ramon, Polyamide desalination membranes: Formation, structure, and properties, Prog. Polym. Sci. 122 (2021) 101451. doi:10.1016/j.progpolymsci.2021.101451.